CHEMPLUSCHEM
COMMUNICATIONS

ChemPubSoc Europe

DOI: 10.1002/cplu.201402109

Structure-Dependent Selective Hydrogenation of α,β-Unsaturated Aldehydes over Platinum Nanocrystals Decorated with Nickel

Zhi Jiang,[a, b] Yonghui Zhao,[a] Lingzhao Kong,[a] Ziyu Liu,[a] Yan Zhu,*[a] and Yuhan Sun*[a]

The shape sensitivity of monometallic Pt and bimetallic Pt–Ni nanocrystals in α,β-unsaturated aldehydes is studied by using a cubic shape enclosed by six {100} facets as well as an octahedral shape surrounded by eight {111} facets. Compared with monometallic Pt and bimetallic Pt–Ni cubic/octahedral shapes, Pt_3Ni cubes enhanced the selective hydrogenation of the C=O double bond and suppressed the selective hydrogenation of the C=C double bond of the α,β-unsaturated aldehyde. The Pt, Pt_3Ni, or PtNi octahedral shape is an unfavorable structure for C=O hydrogenation and enables the activation of the whole conjugated system of the molecule, which leads to complete hydrogenation to form the saturated alcohol product. The synergistic effects of the surface structure and electronic properties of Pt or Pt–Ni nanocrystals play a key role in controlling the selective hydrogenation of C=C and C=O bonds of α,β-unsaturated aldehydes.

Great effort has been made to control the selective hydrogenation of C=O and C=C bonds of α,β-unsaturated aldehydes or ketones for valuable industrial products.[1–5] The difference in bond energy—715 kJ mol^{-1} for the energy of the C=O double bond and 615 kJ mol^{-1} for the C=C double bond—makes the hydrogenation of the C=O bond more difficult than hydrogenation of the C=C bond, yet the resulting unsaturated alcohol products from C=O hydrogenation are valuable intermediates for the production of perfumes and flavorings.[6–9] Selective hydrogenation of α,β-unsaturated aldehydes/ketones is often used as a structure-dependent reaction to investigate the capability of the hydrogenation of C=O and C=C bonds over model catalysts. As we already know, the catalytic activity and selectivity are affected by several factors, including catalyst preparation and activation procedures, the geometric structure of catalysts, as well as the electronic structure of catalysts.[10–15] Therefore, many attempts have been made to promote the hydrogenation of the C=O double bond by taking advantage of the synergistic effects of metallic catalysts, in which bimetallic catalysts with particular geometric and electronic structures display strongly structure-dependent behavior.[16–20] In particular, Pt-based bimetallic nanocrystals such as pure Pt crystals exhibit defined crystallographic planes and can be used to explore the structure sensitivity of liquid-phase reactions.[21–26] Benzene hydrogenation was used as a example to demonstrate that both cyclohexene and cyclohexane formed on cuboctahedral Pt nanoparticles, and only cyclohexane formed on cubic Pt nanoparticles.[27]

In this study, monometallic Pt and bimetallic Pt–Ni (Pt atoms replaced with Ni atoms) nanocrystals with a well-defined cubic shape enclosed by six {100} facets as well as an octahedral shape surrounded by eight {111} facets were synthesized. Herein, the replacement of one atom of every four Pt atoms or two Pt atoms with one Ni atom (referred to as Pt_3Ni and PtNi) can be effectively controlled by the choice of ratios between Pt and Ni precursors. Studies of the hydrogenation of an α,β-unsaturated aldehyde (cinnamaldehyde) were undertaken on the well-defined single-crystal surface of cubic and octahedral shapes to establish the specific modes of adsorption and achieve a better understanding of the mechanism of selective hydrogenation. With respect to monometallic Pt and bimetallic Pt–Ni cubic/octahedral shapes for selective hydrogenation of the α,β-unsaturated aldehyde, Pt_3Ni cubes with six (100) surfaces enhanced the selectivity of C=O bond hydrogenation and suppressed the selectivity of C=C bond hydrogenation, which could be attributed to the modified electronic structure and steric effect on Pt_3Ni cubes through doping of Ni atoms. However, the octahedron with the closed-packed (111) surfaces, regardless of whether it was Pt, Pt_3Ni, or PtNi, was an unfavorable structure for C=O hydrogenation, as it induces a steric hindrance toward the accommodation of the C=O group and enables the activation of the entire conjugated system of the molecule, thus leading to complete hydrogenation to form the saturated alcohol product. Thus, surface, composition, and structure are essential for achieving synergy in terms of catalytic activation of the C=C and C=O bonds of α,β-unsaturated aldehydes/ketones.

Typical transmission electron microscopy (TEM) images of Pt_3Ni shapes are shown in Figure 1. The cubic nanocrystals are less than 10 nm in size and exclusively bound by six {100} facets, as indicated by the continuous lattice fringes with interplanar spacings of 0.185 nm on the basis of high-resolution (HR) TEM analysis (Figure 1b). Energy-dispersive spectrometry (EDS) revealed the coexistence of Pt and Ni in the cubes at an

[a] Z. Jiang, Dr. Y. Zhao, Dr. L. Kong, Dr. Z. Liu, Prof. Y. Zhu, Prof. Y. Sun
CAS Key Laboratory of Low-Carbon Conversion Science and Engineering, Shanghai Advanced Research Institute
Chinese Academy of Sciences, No. 100 Haike Road
Pudong District, Shanghai 201210 (P. R. China)
Fax: (+86) 21-20350867
E-mail: zhuy@sari.ac.cn
sunyh@sari.ac.cn

[b] Z. Jiang
University of Chinese Academy of Sciences
Beijing 100049 (P. R. China)

Supporting information for this article is available on the WWW under http://dx.doi.org/10.1002/cplu.201402109.

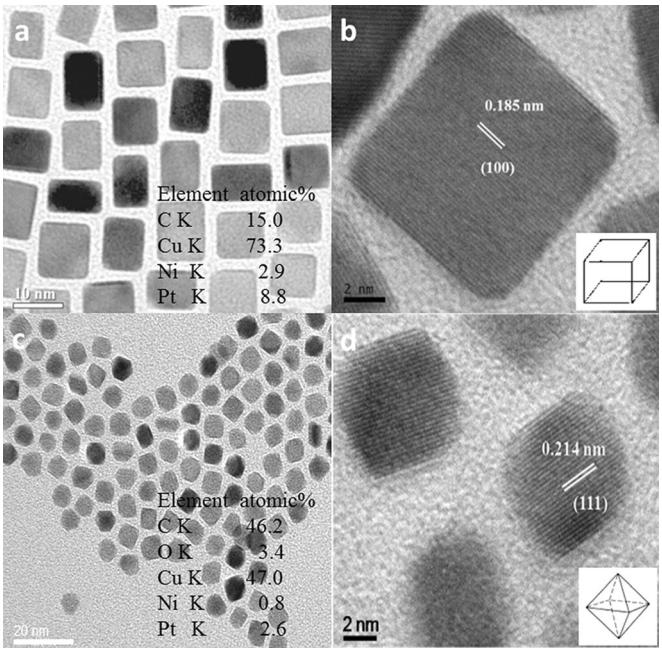

Figure 1. (a) TEM and (b) HRTEM images of Pt_3Ni cubes. (c) TEM and (d) HRTEM images of Pt_3Ni octahedrons. Insets show the atom ratios of Pt and Ni from EDS.

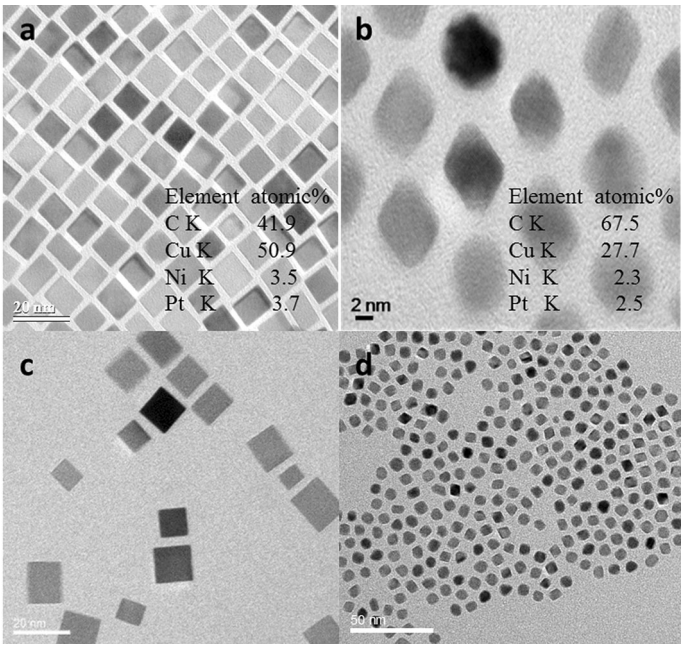

Figure 2. TEM images of (a) PtNi cubes, (b) PtNi octahedrons, (c) Pt cubes, and (d) Pt octahedrons. Insets show the atom ratios of Pt and Ni from EDS.

atomic ratio of about 3:1 (Figure S1a in the Supporting Information). Figure 1c,d shows that the octahedral nanocrystals are uniform in their narrow size distribution (about 5 nm) and exclusively enclosed by eight equivalent {111} facets, which was determined by the crystal lattice fringes being 0.214 nm apart in the HRTEM image (Figure 1d). The atomic ratio of Pt and Ni in the octahedron is about 3:1, as indicated by EDS (Figure S1b). TEM images of monometallic Pt cubes and octahedrons as well as bimetallic PtNi cubes and octahedrons are also shown in Figure 2. The insets in Figure 2a,b show the atomic ratios of Pt and Ni in cubes (1:1) and in the octahedron (1:1), respectively.

The comparisons of the catalytic activity of monometallic Pt and bimetallic Pt–Ni (Pt_3Ni and PtNi) nanocrystals for the selective hydrogenation of α,β-unsaturated aldehydes (cinnamaldehyde) are shown in Figure 3. Although Pt, PtNi, and Pt_3Ni cubes and octahedrons achieved high catalytic activity for the hydrogenation of unsaturated aldehyde, they have different abilities when it comes to selective hydrogenation of C=O and C=C bonds. In terms of cubic nanocrystals, the saturated aldehyde from C=C bond hydrogenation was found before 10 hours of reaction and then transformed to the complete hydrogenation product after 10 hours of reaction. The phenomenon can be also obtained over Pt (Figure 3a), Pt_3Ni (Figure 3c), and PtNi cubes (Figure 3e). Nevertheless, the selectivity towards the unsaturated alcohol from C=O bond hydrogenation was different with cubes. Hydrogenation of only the C=O double bond over monometallic Pt cubes was not achieved. When one-quarter of the Pt atoms were replaced with Ni atoms to form Pt_3Ni cubes, the selectivity of C=O bond hydrogenation was higher than that of C=C bond hydrogenation after 3 hours of reaction (see Figure 3c). When more Pt atoms were replaced with Ni atoms, such as half of the Pt atoms being replaced with Ni atoms to form PtNi cubes, however, hydrogenation of the C=O bond was suppressed and the unsaturated alcohol was a minor product, as shown in Figure 3e.

Interestingly, octahedral nanocrystals including Pt, Pt_3Ni, and PtNi achieved different results to the cubic nanocrystals. As shown in Figure 3b,d,f, hydrogenation of both C=O and C=C bonds was suppressed over Pt and Pt–Ni octahedrons, and saturated alcohol from complete hydrogenation was a major product, although saturated aldehyde was formed during the initial reaction and then disappeared after 5 hours of reaction. The selective hydrogenation of C=O and C=C bonds was not found over the (111) surface of the close-packed octahedral structure, which indicated that the selective hydrogenation of C=O and C=C bonds is independent of the compositions of Pt–Ni with octahedral nanocrystals.

To examine the electronic properties of the catalytically active Pt_3Ni cubes, monometallic Pt and bimetallic Pt–Ni (Pt_3Ni and PtNi) cubes/octahedrons were studied by means of high-resolution X-ray photoelectron spectroscopy (XPS). As shown in Figure 4a, the Pt $4f_{7/2}$ and Pt $4f_{5/2}$ binding energies for the monometallic Pt cubes are 70.9 and 74.2 eV, respectively. Shifts in binding energies were found for both Pt_3Ni and PtNi cubes. The Pt $4f_{7/2}$ and Pt $4f_{5/2}$ binding energies for Pt_3Ni cubes were 0.4 eV higher than the value that is characteristic of Pt cubes. Pt $4f_{7/2}$ and Pt $4f_{5/2}$ binding energies of PtNi cubes shifted to the higher binding energies such as 71.4 and 74.7 eV relative to pure Pt cubes. For the octahedral nanocrystals, as shown in Figure 4b, Pt $4f_{7/2}$ and Pt $4f_{5/2}$ binding energies for Pt_3Ni and PtNi octahedrons were almost consistent with those of pure Pt octahedrons (Pt $4f_{7/2}$ and Pt $4f_{5/2}$ are 71.0 and 74.1 eV, respectively). These results reflect the fact that the electronic proper-

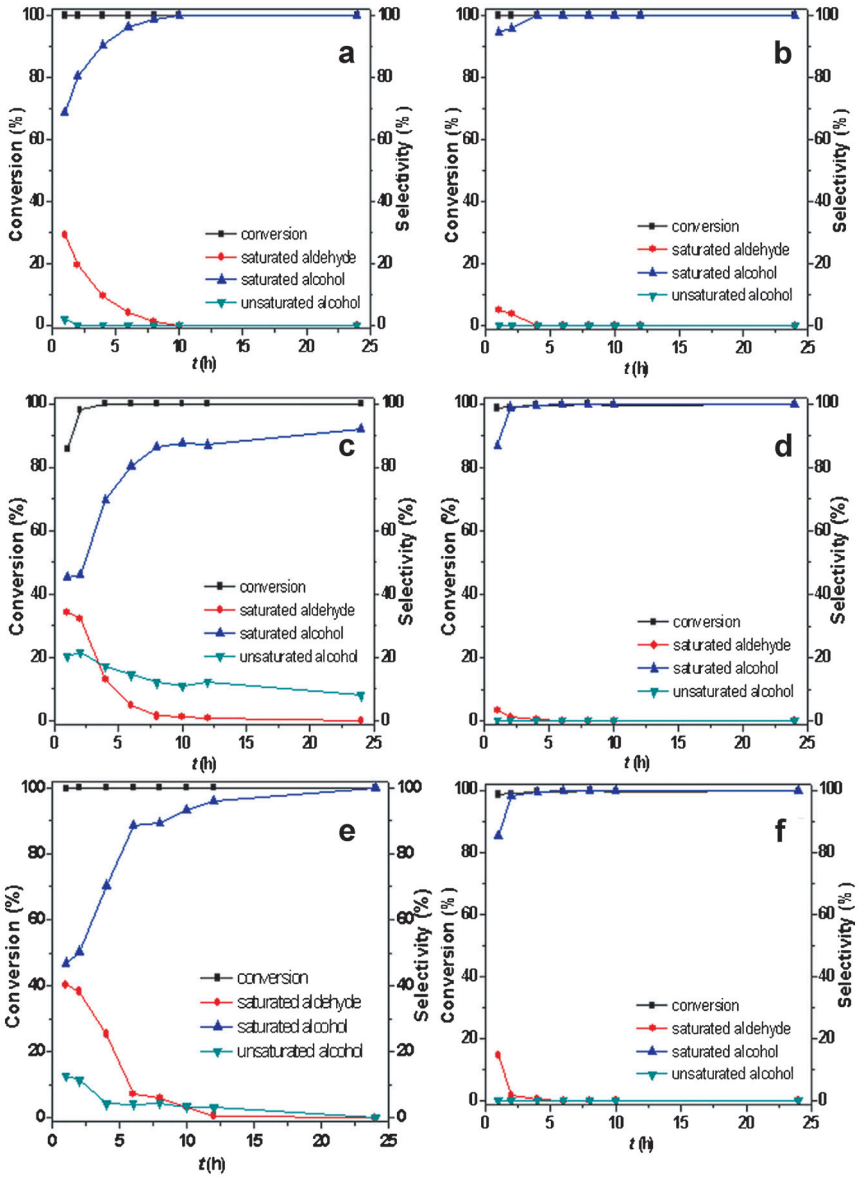

Figure 3. Catalytic performance of (a) Pt cubes, (b) Pt octahedrons, (c) Pt_3Ni cubes, (d) Pt_3Ni octahedrons, (e) PtNi cubes, and (f) PtNi octahedrons for the selective hydrogenation of cinnamaldehyde, respectively.

ties of bimetallic Pt–Ni cubes have been influenced through Ni atoms replacing the Pt atoms of Pt cubes, whereas the charges are not redistributed in Pt_3Ni and PtNi octahedrons even though the Pt atoms of Pt octahedrons are replaced by Ni atoms. Therefore, the electron transfer from the Ni species to the Pt sites evidenced in XPS analysis should explain the promotional effect of Ni in the performance of Pt cubes in terms of the selectivity of C=O and C=C hydrogenation. The high electron density of Pt weakens the strength of the Pt–(C=C) bonding and decreases the activity of the C=C bond through an increase in the repulsive four-electron interaction, and it increases the probability of C=O bond activity attributed to the strength of the Pt(5d)–CO($2\pi^*$) bonding interactions.[3,21,28] It is noted that Pt $4f_{7/2}$ and Pt $4f_{5/2}$ electron binding energies for PtNi cubes were 0.1 eV higher than that of Pt_3Ni cubes, but the selectivity towards C=O bond hydrogenation over PtNi cubes is not higher than that over Pt_3Ni cubes. It suggests that the electronic structure can account for the better selectivity of C=O bond hydrogenation on Pt–Ni cubes than that on Pt–Ni octahedrons, and yet it does not manage to explain why Pt_3Ni cubes favor the activation of the C=O group more than PtNi cubes.

To improve the selectivity of C=O bond hydrogenation and suppress the selectivity of C=C bond hydrogenation, the hydrogenation of C=C step is vital. Density functional theory (DFT) calculations were performed to reveal the origin of the higher reactivity of the cubic shape than octahedral-shaped Pt_3Ni in suppressing the selectivity of C=C bond hydrogenation. $Pt_3Ni(100)$ and $Pt_3Ni(111)$ surfaces were modeled by using 3×3 and 2×2 super cells with three layers of thickness. A vacuum region of 13 Å was considered to avoid electronic interaction between slabs. In the calculations, the bottom layer of metal atoms was fixed and the top two layers and the adsorbates were relaxed. The adsorption energy was defined as $E_{ads} = E_{adsorbate/slab} - E_{adsorbate} - E_{slab}$, in which E_{ads} is the calculated adsorption energy, $E_{adsorbate/slab}$ is the energy of the adsorbed system, $E_{adsorbate}$ is the energy of adsorbate in the gas phase, and E_{slab} is the surface energy. The most stable configurations of C_6H_5-CH-CH_2-CH_2OH on the $Pt_3Ni(100)$ and $Pt_3Ni(111)$ surfaces obtained from our DFT calculations are shown in Figure 5a,b, and the corresponding binding energies are −3.81 and −2.18 eV, respectively. At the same time, the DFT results of H and C_6H_5-CH=CH-CH_2OH and selected geometric parameters are shown in Table S1 of the Supporting Information. The adsorption energy indicates higher binding energy on the $Pt_3Ni(100)$ surface than on the $Pt_3Ni(111)$ surface, which is due to the more open surface structure of the (100) surface than the (111) surface. After obtaining the adsorbed structures of the intermediates, we have further calculated the elementary step related to the formation of C_6H_5-CH-CH_2-CH_2OH. Figure 6 shows the pathway to produce C_6H_5-CH-CH_2-CH_2OH on the $Pt_3Ni(100)$ surface (in red) and $Pt_3Ni(111)$ surface (in black). The located initial states (IS) and transition states (TS) are shown in Figures S2

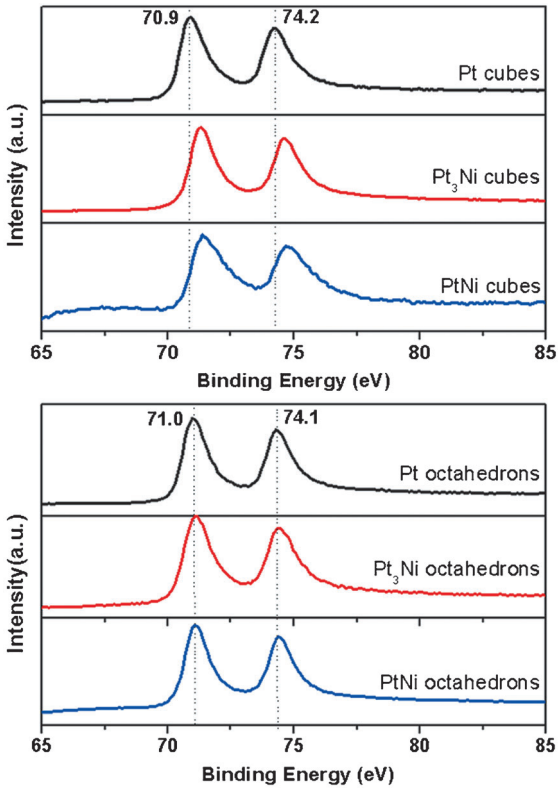

Figure 4. XPS Pt 4f spectra of (a) cubes and (b) octahedrons of Pt, Pt_3Ni, and PtNi.

and S3 of the Supporting Information, respectively. The higher hydrogenation barrier on the (100) plane might be caused by the different adsorption configuration of C_6H_5-CH=CH-CH_2OH. On the $Pt_3Ni(100)$ surface, the CH_2OH group is bonded with the surface with an O-to-surface distance of about 2.08 Å, whereas CH_2OH does not bond with the surface with a longer

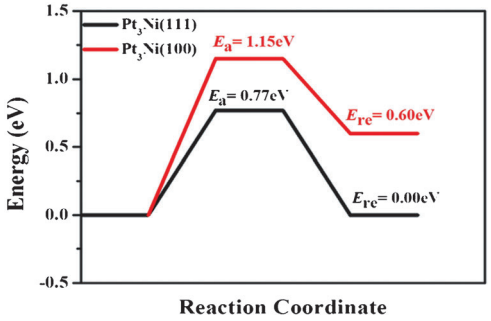

Figure 6. Comparison of the calculated energy profiles for C_6H_5-CH=CH-$CH_2OH + H \rightarrow C_6H_5$-CH-$CH_2$-$CH_2OH$ on the $Pt_3Ni(100)$ surface (in red) and $Pt_3Ni(111)$ surface (in black).

O-to-surface distance (3.18 Å) on the $Pt_3Ni(100)$ surface. As in the case of the $Pt_3Ni(100)$ surface, during the reaction, the adsorption mode results in a longer distance between H and C_6H_5-CH=CH-CH_2OH (3.03 versus 2.64 Å) in the IS and results in a further increase in the activation barrier to produce C_6H_5-CH-CH_2-CH_2OH relative to the $Pt_3Ni(111)$ surface. Thus, our DFT results suggest that the cubic shape could achieve higher selectivity of C=O bond hydrogenation than octahedrally shaped Pt_3Ni.

In summary, the influence of replacing Pt atoms with Ni atoms on cubes is more significant in the selectivity for α,β-unsaturated aldehyde hydrogenation than that on octahedrons. Both monometallic Pt and bimetallic Pt–Ni octahedrons gave similar results for cinnamaldehyde hydrogenation. For cubes, selectivity towards C=O bond hydrogenation is enhanced as Pt atoms on cubes are replaced with Ni atoms, and replacing one-quarter of the Pt atoms with Ni atoms (Pt_3Ni cubes) achieved higher selectivity toward C=O hydrogenation than replacing half of the Pt atoms with Ni atoms (PtNi cubes). Thus, the synergistic effects of the surface structure and electronic properties of nanocrystals are essential in achieving selective hydrogenation of the C=C and C=O bonds of α,β-unsaturated aldehyde/ketone. Overall, this study might raise interesting possibilities for the development of decorated, doped, or replaced nanostructures with well-defined crystal surfaces in heterogeneous catalysis.

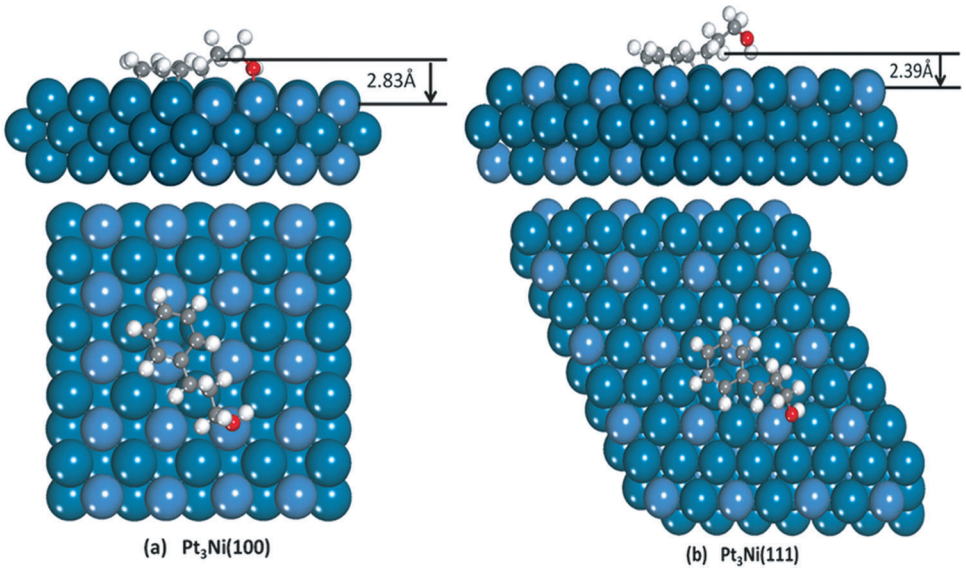

Figure 5. Top and side views of calculated adsorption structures of C_6H_5-CH-CH_2-CH_2OH on (a) $Pt_3Ni(100)$ and (b) $Pt_3Ni(111)$ surfaces.

Experimental Section

Synthesis of Pt_3Ni cubes

In a typical synthesis, under argon flow, platinum acetylacetonate [$Pt(acac)_2$] (20.0 mg, 0.05 mmol), nickel acetylacetonate [$Ni(acac)_2$] (10.0 mg, 0.039 mmol), oleylamine (9 mL), and oleic acid (1 mL) were mixed in a 25 mL three-necked,

round-bottomed flask with a magnetic stirrer. The flask was immersed in an oil bath at 130 °C, and the reaction mixture turned into a transparent yellowish solution. The flask was transferred to a second oil bath at 210 °C under carbon monoxide gas and was injected with methanol (50 μL). The typical flow rate of CO gas was set at 280 mL min^{-1}, and the reaction time was 20 min. The product was precipitated by ethanol and then redispersed in cyclohexane.

PtNi cubes were prepared from [Pt(acac)$_2$] and [Ni(acac)$_2$] as the precursors (the mole ratio of Pt and Ni precursors was 1:0.4) under otherwise identical experimental conditions. Pt cubes were prepared from the [Pt(acac)$_2$] precursor under otherwise identical experimental conditions.

Synthesis of Pt_3Ni octahedrons

Under argon flow, [Pt(acac)$_2$] (20.0 mg, 0.05 mmol), [Ni(acac)$_2$] (4.0 mg, 0.016 mmol), oleylamine (9 mL), and diphenyl ether (1 mL) were mixed in a 25 mL three-necked, round-bottomed flask with a magnetic stirrer. The flask was immersed in an oil bath at 130 °C, and the reaction mixture turned into a transparent yellowish solution. The flask was transferred to a second oil bath at 210 °C under carbon monoxide gas. The rest of the steps followed the same synthetic procedure.

PtNi octahedrons were prepared from [Pt(acac)$_2$] and [Ni(acac)$_2$] as the precursors (the mole ratio of Pt and Ni precursors was 5:4) under otherwise identical experimental conditions. Pt octahedrons were prepared from the [Pt(acac)$_2$] precursor under otherwise identical experimental conditions.

Catalytic test

The catalytic hydrogenation reaction was performed in a stainless steel stirred autoclave with a volume of 100 mL. The dried catalyst (10 mg), alcohol (40 mL), cinnamaldehyde (200 μL), and *n*-dodecane (100 μL, as an internal standard) were mixed in the autoclave. After the autoclave was sealed, H_2 was charged four times to replace air. The autoclave was heated to the reaction temperature of 60 °C in 10 min and H_2 was charged to a final pressure of 2.0 MPa. The hydrogenation reaction was begun by turning on the stirring button. The samples were periodically withdrawn from the reactor and analyzed offline with a gas chromatograph.

Characterization

TEM and HRTEM images were recorded with a JEOL JEM-2100 electron microscope. XPS experiments were carried out with an RBD upgraded PHI-5000C ESCA system (Perkin–Elmer) with $Mg_{K\alpha}$ ($h\nu$ = 1253.6 eV) or $Al_{K\alpha}$ radiation ($h\nu$ = 1486.6 eV). The catalytic products were analyzed with a Shimadzu GC-2014 instrument equipped with a flame ionization detector.

Acknowledgements

This study was supported by the National Natural Science Foundation of China (21273151) and the Shanghai Pujiang Program (13J1407700).

Keywords: bimetallic catalysts · electronic structure · hydrogenation · nickel · platinum

[1] S. Galvagno, C. Milone, A. Donato, G. Neri, R. Pietropaolo, *Catal. Lett.* **1993**, *17*, 55–61.
[2] J. L. Margitfalvi, A. Tompos, I. Kolosova, J. Vaylon, *J. Catal.* **1998**, *174*, 246–249.
[3] R. Hirschl, F. Delbecq, P. Sautet, J. Hafner, *J. Catal.* **2003**, *217*, 354–366.
[4] D. Loffreda, F. Delbecq, V. Fabienne, P. Sautet, *Angew. Chem.* **2005**, *117*, 5413–5416; *Angew. Chem. Int. Ed.* **2005**, *44*, 5279–5282.
[5] L. E. Murillo, C. A. Menning, J. G. Chen, *J. Catal.* **2009**, *268*, 335–342.
[6] V. Ponec, *Appl. Catal. A* **1997**, *149*, 27–48.
[7] P. Clause, *Topics Catal.* **1998**, *5*, 51–62.
[8] U. K. Singh, M. A. Vannice, *Appl. Catal. A* **2001**, *213*, 1–24.
[9] Y. Wu, S. F. Cai, D. S. Wang, W. He, Y. D. Li, *J. Am. Chem. Soc.* **2012**, *134*, 8975–8981.
[10] F. Delbecq, P. Sautet, *J. Catal.* **1996**, *164*, 152–165.
[11] M. Consonni, D. Jokic, D. Y. Murzin, R. Touroude, *J. Catal.* **1999**, *188*, 165–175.
[12] F. Y. Zhao, Y. Ikushima, M. Shirai, T. Ebina, M. Arai, *J. Mol. Catal.* **2002**, *180*, 259–265.
[13] P. Mäki-Arvela, J. Hájek, T. Salmi, D. Y. Murzin, *Appl. Catal. A* **2005**, *292*, 1–49.
[14] L. E. Murillo, A. M. Goda, J. G. Chen, *J. Am. Chem. Soc.* **2007**, *129*, 7101–7105.
[15] Y. Zhu, H. F. Qian, B. A. Drake, R. C. Jin, *Angew. Chem.* **2010**, *122*, 1317–1320; *Angew. Chem. Int. Ed.* **2010**, *49*, 1295–1298.
[16] C. G. Raab, J. A. Lercher, *J. Mol. Catal.* **1992**, *75*, 71–79.
[17] M. Lucas, P. Claus, *Chem. Eng. Technol.* **2005**, *28*, 867–870.
[18] J. Silvestre-Albero, J. C. Serrano-Ruiz, A. Sepulveda-Escribano, F. Rodriguez-Reinoso, *Appl. Catal. A* **2005**, *292*, 244–251.
[19] J. G. Chen, S. T. Qi, M. P. Humbert, C. A. Menning, Y. X. Zhu, *Acta. Phys. Chim. Sin.* **2010**, *26*, 869–876.
[20] J. Y. Park, Y. W. Zhang, M. Grass, T. F. Zhang, G. A. Somorjai, *Nano Lett.* **2008**, *8*, 673–677.
[21] N. Mahata, F. Goncalves, M. Fernando R. Pereira, J. L. Figueiredo, *Appl. Catal. A* **2008**, *339*, 159–168.
[22] D. Xu, S. B. Liznakov, Z. P. Liu, J. Y. Fang, N. Dimitrov, *Angew. Chem.* **2010**, *122*, 1304–1307; *Angew. Chem. Int. Ed.* **2010**, *49*, 1282–1285.
[23] J. B. Wu, J. L. Zhang, Z. M. Peng, S. C. Yang, F. T. Wagner, H. Yang, *J. Am. Chem. Soc.* **2010**, *132*, 4984–4985.
[24] L. Gan, M. Heggen, S. Rudi, P. Strasser, *Nano. Lett.* **2012**, *12*, 5423–5430.
[25] Y. J. Kang, J. B. Pyo, X. C. Ye, T. R. Gordon, C. B. Murray, *ACS Nano* **2012**, *6*, 5642–5647.
[26] Y. J. Kang, X. C. Ye, J. Cai, R. E. Diaz, R. R. Adzic, E. A. Stach, C. B. Murry, *J. Am. Chem. Soc.* **2013**, *135*, 42–45.
[27] K. M. Bratlie, H. Lee, K. Komvopoulos, P. D. Yang, G. A. Somorjai, *Nano Lett.* **2007**, *7*, 3097–3101.
[28] F. Ammari, J. Lamotte, R. Touroude, *J. Catal.* **2004**, *221*, 32–42.

Received: April 14, 2014
Revised: June 17, 2014
Published online on July 17, 2014